2006-07

A microtexture investigation of recrystallization during friction stir processing of as-cast NiAl bronze

Oh-Ishi, Keiichiro; Zhilyaev, Alexander P.; McNelley, Terry R.

Elsevier

K. Oh-Ishi, A.P. Zhilyaev, T.R. McNelley, "A microtexture investigation of recrystallization during friction stir processing of as-cast NiAl bronze," Metallurgical and Materials Transactions A, v. 37A, (July 2006), pp. 2240-2251.
http://hdl.handle.net/10945/55872

A Microtexture Investigation of Recrystallization during Friction Stir Processing of As-Cast NiAl Bronze

KEIICHIRO OH-ISHI, ALEXANDER P. ZHILYAEV, and TERRY R. McNELLEY

As-cast NiAl bronze (NAB) was subjected to friction stir processing (FSP). Orientation imaging microscopy (OIM) methods were used to obtain microtexture data in the stir zone (SZ) and along its periphery. At selected SZ locations, orientation data were obtained by convergent beam electron diffraction (CBED) methods in transmission electron microscopy (TEM). Random α phase textures were apparent in the SZ. The α grains tended to be equiaxed, exhibited annealing twins, and were refined to 1 to 2 μm at the edge of the SZ. The population of subgrain boundaries in α phase grains was highest near the plate surface in contact with the tool and decreased with depth in the SZ, reflecting deformation by the tool shoulder after the passage of the tool pin. Distinct shear texture components were apparent in the thermomechanically affected zone (TMAZ) outside of and along the periphery of the SZ. A texture gradient from the TMAZ into the SZ was apparent and was steeper on the advancing side and under the SZ center than on the retreating side. The apparent shear plane tended to align with the local interface between the SZ and TMAZ, while the shear direction tended to align with the FSP traversing direction. In this material, the SZ–TMAZ interface is a distinct boundary between recrystallized and deformed regions and the α-phase grain refinement reflects dynamic recrystallization and, in locations near the SZ–TMAZ interface, particle-stimulated nucleation (PSN) at undissolved Fe_3Al particles.

I. INTRODUCTION

FRICTION stir processing (FSP) is an adaptation of friction stir welding (FSW), a solid-state joining process originally developed at The Welding Institute.[1] Friction stir processing enables localized modification and control of microstructures in near-surface layers of metallic components.[2,3,4] In the process, a cylindrical, wear-resistant tool consisting of a smaller diameter pin with a concentric, larger-diameter shoulder is rotated and forced into the surface of the work piece. As the tool penetrates, a combination of frictional and adiabatic heating softens the material so that tool rotation induces a stirring action and flow of material about the pin. The severe, but localized, plastic deformation results in formation of a stir zone (SZ), while adjacent regions that experience only moderate straining comprise the thermomechanically affected zone (TMAZ). Large areas may be processed by traversing the tool in a pattern on the work piece surface.

Friction stir processing has been employed to homogenize and refine microstructures in both cast and wrought metals, including alloys of Al[5–10] and Mg[11,12] and higher melting alloys of Cu,[13] Fe,[14] and Ti.[15] Benefits of FSP in cast metals include elimination of porosity and local conversion of cast microstructures to a wrought condition, with enhanced near-surface properties. Significantly improved strength/ductility combinations[16,17] and high-strain-rate superplasticity[3–7,18] have been achieved by FSP of wrought materials. Depending on alloy constitution and prior history, the FSP thermomechanical cycle will induce various restoration and transformation processes that will be reflected in SZ and TMAZ microstructures. However, the direct measurement of temperatures, strains, and strain rates in these regions is difficult due to steep gradients and transients in these quantities, and this is an impediment in the assessment of processing-induced microstructures.

Quantitative microstructure analysis following FSP of the cast NAB materials of interest here has been used to develop estimates of local peak SZ temperatures. The estimates have relied mainly on assessment of the transformation products of the β phase observed in the microstructure of processed material. Details of the estimation procedure have been given in previous reports.[19,20] Briefly, during cooling at rates $\sim 10^{-3}$ °C s^{-1} after casting, the NAB solidifies as a single-phase β bcc solid solution. At about 1030 °C, the primary α begins to form with Widmanstätten morphology in the β. At 930 °C, the globular precipitate, κ_{ii}, which is nominally Fe_3Al having a DO_3 structure, starts to form in the remaining β and may attain sizes of 20 to 30 μm, while, upon cooling below 860 °C, a finer Fe_3Al precipitate, κ_{iv}, begins to form in the primary α. The volume fraction of β continues to decrease until the eutectoid reaction, $\beta \rightarrow \alpha + \kappa_{iii}$, takes place at ~800 °C. The κ_{iii} is nominally NiAl having a B2 structure. Thus, following such equilibrium cooling, the microstructure of the as-cast NAB consists of a primary α fcc terminal solid solution, which contains a fine dispersion of κ_{iv} precipitate particles, and a eutectoid constituent, $\alpha + \kappa_{iii}$, which contains coarse, globular κ_{ii} particles.

After FSP, SZ microstructures in NAB materials generally include primary α, nonequilibrium transformation products of the β phase, κ_{ii}, and, in some locations, κ_{iv}. These microstructures depend strongly on local peak temperatures and subsequent cooling rates. Altogether, the absence of the $\alpha + \kappa_{iii}$ eutectoid constituent as well as the presence of nonequilibrium β transformation products, including fine Widmanstätten α, bainite, and martensite,

KEIICHIRO OH-ISHI, Postdoctoral Associate, is with the National Institute for Materials Science, Ibaraki 305-0047, Japan. ALEXANDER P. ZHILYAEV, NRC Senior Research Associate, and TERRY R. McNELLEY, Distinguished Professor, are with the Department of Mechanical and Astronautical Engineering, Naval Postgraduate School, Monterey, CA 93943-5146. Contact e-mail: tmcnelley@nps.edu

Manuscript submitted October 14, 2005.

indicate local heating to temperatures above the eutectoid (~800 °C). The relative fractions of the primary α, the β transformation products, and the κ_{ii} and κ_{iv} were employed to estimate local peak temperatures in conjunction with data on phase equilibria in NAB alloys. These estimates assume local equilibrium due to acceleration of diffusion-controlled reactions by excess vacancy generation during deformation and heating to the local peak temperature.[21,22,23] Various morphologies of the primary α and the β transformation products have been observed. These morphologies apparently depend on the details of the local thermomechanical history, but also suggest that the α and β phases experience compatible deformation during straining at $T \geq 800$ °C. Detailed discussions of the β transformation products that form during cooling after passage of the tool have already been provided.[19,20] These transformation products obscure the mechanisms of microstructure evolution that occurred within the β during its deformation at elevated temperature during FSP. However, the effects of deformation, recovery, recrystallization, and growth within the primary α are retained after FSP, and these processes are the subject of the present report.

Sato *et al.*[24] have observed shear textures at the center of an FSW zone in AA6063 material; the textures exhibited two characteristic orientations. These orientations had a pair of common {111} and <110> aligned parallel to the pin surface and transverse direction of the plate. Such inclination of the {111} slip planes in shear textures has been reported to appear from locations under the shoulder to points at the midplane in the weld zone.[25] Fonda *et al.*[26] have also correlated observed lattice orientations in FSW of AA2195, an Al-Cu-Li alloy, with shear texture components having {111} aligned with the pin surface. They also reported that these shear textures were present throughout the weld zone, and they concluded that refined grains had formed by processes of grain subdivision and the recovery-dominated evolution of high-angle boundaries by dislocation accumulation. Park *et al.*[27] have conducted FSW of hcp Mg. They showed that the (0002) basal plane, which is the preferred slip plane in Mg, becomes aligned with an ellipsoidal surface in the nugget-shaped SZ.

The high stacking fault energy of Al and its alloys leads to a predominance of recovery during severe deformation at elevated temperatures, and this is likely reflected in the development and persistence of deformation textures throughout the SZ. Nevertheless, such recovery dominated processes may lead to the formation of refined grains and high-angle boundaries, although the details of the dislocation reactions leading to formation of the high-angle grain boundaries remain to be clarified. In contrast, Cu and its alloys are moderate or low stacking fault energy materials. In this case, recrystallization *via* formation and long-range migration of high-angle boundaries typically occurs after sufficient deformation, or may occur dynamically during elevated temperature deformation. Such recrystallization processes generally result in the replacement of deformation textures with recrystallization textures, although such texture changes depend on alloy constitution and processing conditions. Accordingly, it is anticipated that recrystallization may become apparent in the SZ and surrounding areas for NAB materials that have been subjected to FSP, and this will be reflected in the resulting SZ textures.

The objectives of the current investigation are twofold. The first is to assess α phase microstructures and microtextures throughout the SZ and surrounding TMAZ by means of OIM and TEM, as well as conventional microscopy methods. The second is to evaluate the restoration mechanisms in this phase and determine the role of alloy constitution in the processes of recovery and recrystallization in the α. The roles of the α/β interfaces and constituent particles will be of particular interest in this regard.

II. EXPERIMENTAL PROCEDURES

Details of the composition of the material examined here have been included in previous reports;[19,20] the NAB specification corresponds to UNS C95800, which is nominally Cu-9Al-5Ni-4Fe-1Mn (wt pct). Friction stir processing was accomplished at the Rockwell Scientific Company (Thousand Oaks, CA) with tools machined from MP159, an alloy having a nominal composition of 25Ni-36Co-19Cr-9Fe-7Mo-3Ti (wt pct). Details of the tool design have also been given previously;[19,20] briefly, the tools had a shoulder diameter of 23.8 mm, a pin diameter of 7.95 mm, and a pin depth of 6.65 mm. Additionally, the pin had a spiral groove. Two processing conditions from prior work were selected for the current study. These were (1) tool rotation and traversing rates of 800 rpm and 152 mm m^{-1} (6 in m^{-1}), respectively; and (2) rotation and traversing rates of 1000 rpm and 203 mm m^{-1} (8 in m^{-1}). In both cases, the tool axis was inclined ~3 deg opposite to the direction of tool advance and the process involved a single traverse approximately 200 mm in length under *X*-axis displacement rate control. The ratio of the traversing rate to the rotation rate, *i.e.,* tool advance per revolution (Table I; the designators are only serial numbers), is essentially the same for these two samples; accordingly, the SZ microstructures are similar and have been discussed in previous reports.[19,20] The conventional axes for FSP are included in the schematic of Figure 1; the tool moves in the *X* direction, *Y* is the transverse direction, and *Z* is the plate normal. In Figure 1, the *Y-Z* plane is the transverse plane; here, a plan view of the SZ was obtained in a plane parallel to the *X-Y* plane but located 2.5 mm below the plate surface.

Samples for optical microscopy (OM) were prepared either by sectioning on a transverse plane or on the plane of the plan view. In both cases, the sectioning was conducted at a location approximately at the midpoint of the traverses where the FSP appeared to be at a steady state. The OM involved standard preparation methods that have been described previously.[19,20] Etched samples were examined using bright-field (BF) illumination in a Zeiss JENAPHOT* 2000 equipped with a digital imaging system.

*JENAPHOT is a trademark of Carl Zeiss, Oberkochen, Germany.

Table I. Processing Parameters and Tool Advance Per Revolution for Samples Examined in This Study

Process Designator	Rotation Rate (rpm)	Traversing Rate (mm m^{-1})	Tool Advance per Revolution (mm/rev)
FSP516	800	152	0.191
FSP520	1000	203	0.203

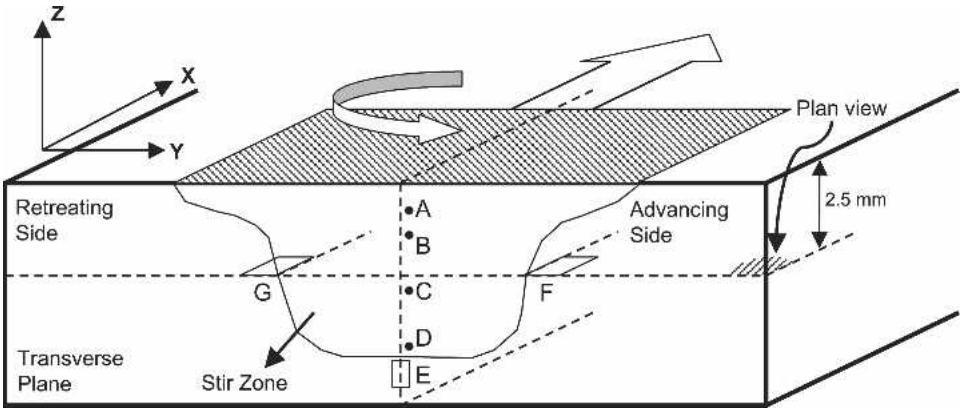

Fig. 1—Schematic diagram of material after FSP, indicating planes of sectioning and the regions examined in the current study. The definition of axis is indicated in the inset; the tool traversing direction is *X*, the longitudinal direction is *Y*, and the plate normal direction is *Z*.

Transmission electron microscopy (TEM) was accomplished with a TOPCON** 002B microscope equipped with a LaB_6 filament and operated at 200 kV. Samples for TEM examination were obtained by first sectioning with a low-speed diamond saw to obtain a transverse slice through the SZ of processed material. Then, disks 3 mm in diameter and having normal directions parallel to the travel direction were thinned to perforation by electropolishing using a 33 pct nitric acid–67 pct methanol solution initially cooled to –25 °C. Convergent-beam electron diffraction (CBED) patterns were taken from each α phase grain in a region of contiguous grains, and the patterns were then analyzed to determine unambiguous lattice orientations of the grains. The orientation of the CBED pattern captured from each grain was indexed with an accuracy of ~0.2 deg using the Tools for Orientation Crystallographic Analysis (TOCA) software (EDAX-TSL, Inc., East Mahway, NJ) for TEM. The grain-to-grain lattice disorientation accuracy was then ~0.4 deg.

**TOPCON is a trademark of Topcon America Corp., Paramus, NJ.

Microtexture analysis by orientation image microscopy (OIM) was conducted using a Topcon SM-510 scanning electron microscope (SEM) equipped with a tungsten filament and operated at 20 kV. The OIM samples were prepared from the same two planes, *i.e.*, the transverse plane and the plan-view plane (Figure 1), and were electropolished after the same standard polishing preparation as for OM. The OIM software is designed to accept input data for multiple phases in order to enable separate indexing of electron backscatter diffraction (EBSD) patterns for each phase. In the as-cast NAB alloy, the primary α is fcc, the fine κ_{iv} and coarse globular κ_{ii} are both $D0_3$, and the κ_{iii} in the eutectoid constituent is B2.[28,29,30] Here, the B2 and $D0_3$ structures have interatomic spacings that differ by less than 1 pct and therefore would be expected to exhibit essentially identical EBSD patterns. In fact, EBSD patterns were obtained from the coarse globular particles in the present work, but it was not possible to distinguish the lattice as either B2 or $D0_3$, and energy-dispersive spectrometry (EDS) would be required in order to distinguish these phases. The fine κ_{iv} particles were near or below the resolution of OIM. Furthermore, during FSP of the as-cast NAB, the β phase forms by the reversion reaction $\alpha + \kappa_{iii} \rightarrow \beta$ at temperatures >~800 °C; although the β phase has a bcc structure at the high temperature, various transformation products of β form during rapid cooling following passage of the tool.[19,20] These transformation products may include fine bainitic or martensitic constituents in prior β regions that also cannot be resolved by OIM. Accordingly, OIM data were obtained for areas $100 \times 100\ \mu m^2$ in size using a step size of 1 μm and the orientation data from the fcc α phase were of primary concern here.

III. RESULTS

A. *Inside of the SZ*

Figure 2 shows OIM data from the locations along the vertical traverse through the SZ center on the transverse plane in FSP516. The data in Figures 2(a) through (d) correspond approximately to locations A through D in the schematic in Figure 1; *i.e.,* they represent locations from ~1 mm below the surface in contact with the tool to a location ~5 mm below this surface and near the boundary of the SZ. These data are in the form of image-quality (IQ) maps, discrete (001) and (111) pole figures, and histograms representing the grain-to-grain misorientation angle distributions in the α phase. Detailed OM and TEM analyses of the β transformation products at these SZ locations for the processing conditions of Table I have been previously reported by the authors.[19] Here, higher IQ in the EBSD patterns corresponds to brighter gray tones in the maps; the corresponding areas in the maps are mainly the primary α that persisted during processing. Locations of low IQ during scanning may reflect locations near α-phase grain boundaries, undissolved κ_{ii}, or fine, complex β transformation products. The banded distribution of primary α and β transformation products apparent in Figures 2(a) through (c) agrees with previous OM analysis of this same material.[19] Also, grain size in the primary α becomes finer with depth in the SZ and is finest at the bottom (Figure 2(d)) of the SZ. In upper regions of the SZ in Figures 2(a) and (b), Widmanstätten α is apparent in the dark regions between the bands of primary α; the Widmanstätten α typically forms from prior β in regions heated to $T >$ ~900 °C during processing.[19,20]

At all SZ locations, the discrete pole figure data show only random orientations in the α phase, in contrast to

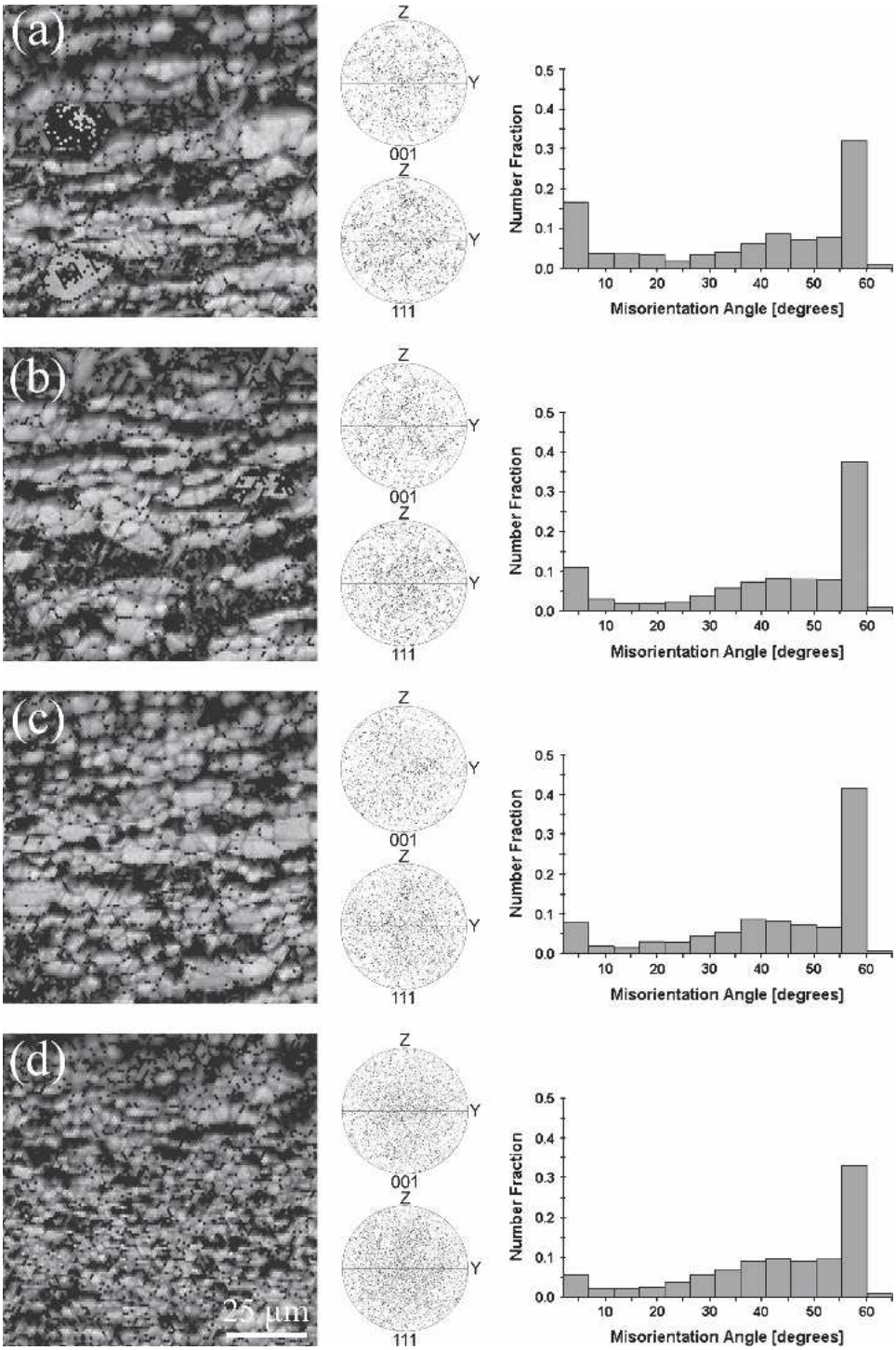

Fig. 2—OIM results for regions along a vertical traverse through the center of the SZ on the transverse cross section of FSP516 (locations A through D in Figure 1), in the form of IQ maps, misorientation angle distributions, and discrete (001) and (111) pole figures.

observations of distinct shear textures in the SZ in FSP/W of aluminum alloys.[24–26,31] The observation here of random textures within the SZ is indicative of recrystallization involving the formation of randomly oriented grain nuclei followed by the long-range migration of high-angle boundaries during the thermomechanical cycle of FSP. The distributions of grain-to-grain misorientation angles for all locations show a distinct random component, which is similar to that predicted by MacKenzie for randomly oriented cubes,[32] but with additional peaks at 0 to 5 deg and at 60 deg. Examination of these data shows that the population of the low-angle boundaries (0 to 5 deg) is highest at locations nearest the plate surface in contact with the tool shoulder. These low-angle boundaries may reflect deformation of newly recrystallized grains by the tool shoulder after passage of the tool pin. At all SZ locations, there is a

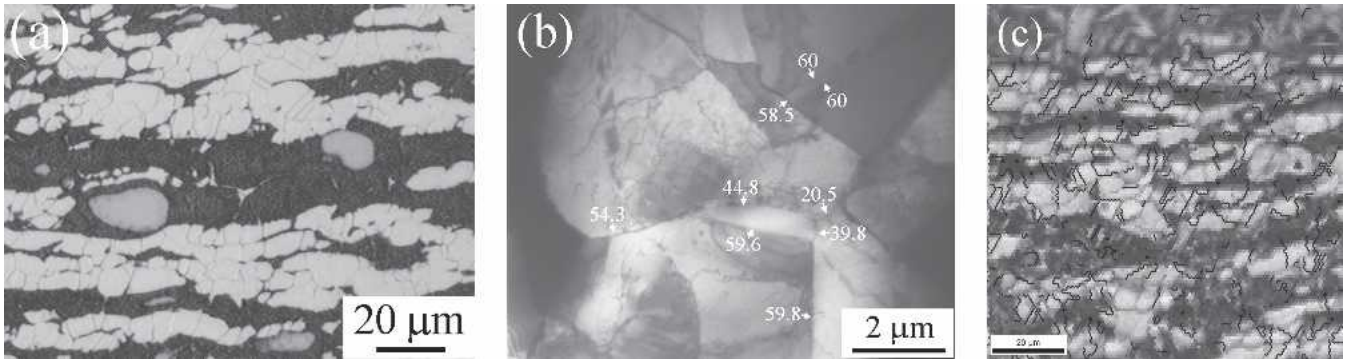

Fig. 3—Detailed microscopy results corresponding to the location of Figure 2(b): (*a*) optical micrographs showing bandlike structures consisting of α phase and β transformation products and (*b*) TEM micrograph showing fine grains with high-angle boundaries in the α grains. Grain-to-grain misorientation angles were obtained by CBED methods and TOCA analysis; boundaries over 15 deg are indicated in the image. (*c*) Boundaries of 55 to 62.8 deg disorientation are indicated by the superimposed black lines in the IQ grain map for location B.

distinct population of ~60 deg boundaries that likely reflects the formation of annealing twins after recrystallization during FSP.

Figure 3(a) is an optical micrograph from location B, *i.e.,* Figure 2(b), showing that the structure consists of alternating bands of primary α (light etching) and β transformation products (dark etching) that are elongated in the horizontal (*Y*) direction. The primary α bands consist of equiaxed grains and numerous twins are also apparent. The κ_{iv} phase that was present in the primary α in as-cast material is not apparent in this image. The dark-etching bands comprise a mixture of bainite, martensite, and small amounts of Widmanstätten α; these constituents are transformation products formed during rapid cooling from the β phase.[19] Globular particles of the κ_{ii} phase are also present in the prior β. Along with the relative fractions of primary α and β transformation products, these observations indicate that the local peak temperature was ~930 °C at this location during FSP.[19] Figure 3(b) shows a TEM image from the primary α at this location; dislocations and numerous subgrain boundaries are evident. Grain-to-grain disorientation angles determined by TOCA have been superimposed for those boundaries of disorientation >15 deg. Straight boundaries of annealing twins having disorientation angles of ~60 deg are apparent in several locations. The data of Figure 3(b) are consistent with the formation of refined grains at the high local temperature during FSP, followed by moderate deformation and subsequent annealing of these grains. The boundaries of 55 to 62.8 deg disorientation in the IQ map of Figure 2(b) are indicated by superimposed black lines in Figure 3(c). A comparison suggests that the black lines in Figure 3(c) correspond to the annealing twins in the optical micrograph of Figure 3(a), and rotation axis data for these boundaries indicate that almost all of them correspond closely to the 60 deg/<111> first-order twin relationship in fcc metals.[33]

The results of TEM/TOCA analysis for a location near the boundary of the SZ under the tool pin are shown in Figure 4. This location, D, corresponds to that in Figure 2(d). Figure 4(a) is a TEM image suggesting that highly refined α grains 1 to 2 μm in size are attained in this location by processing. The boundaries in this image are shown in the tracing of the boundaries in Figure 4(b) in which the line width corresponds to the grain-to-grain disorientation angles from TOCA analysis. The hatched areas indicate locations comprising either κ_{ii} or κ_{iv} constituent particles that were deformed or broken up by processing. Most of the boundaries are of high disorientation angle, $\theta > 40$ deg; these are indicated by the thickest lines, and many of these are twin boundaries of approximately 60 deg misorientation.

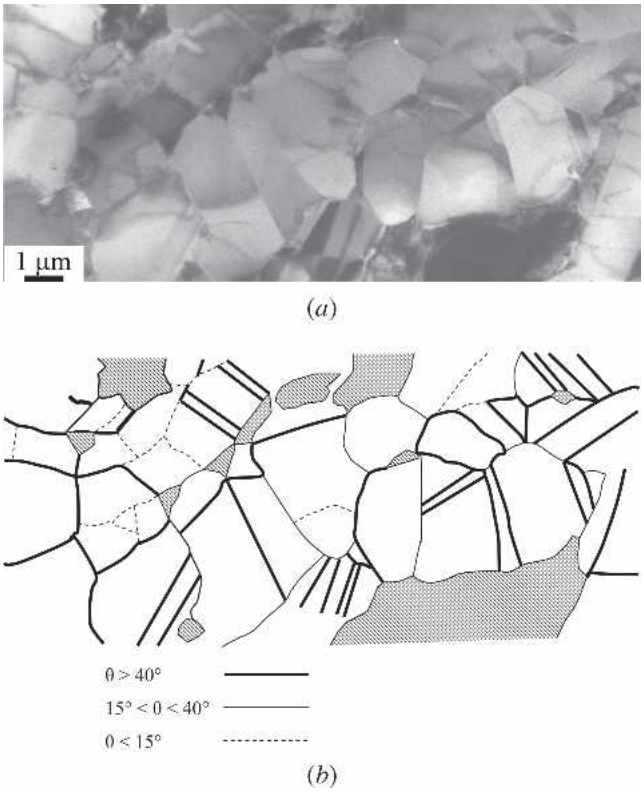

Fig. 4—(*a*) A refined grain structure is shown in a montage of TEM images. (*b*) Results of CBED analysis by TOCA in the lower SZ corresponding to location D in Figure 1. Grain boundaries are delineated by various lines depending upon the grain-to-grain disorientation angle; thick for $\theta > 40$ deg, thin for 15 deg $< \theta <$ 40 deg, and dotted for $\theta < 15$ deg.

Fig. 5—A montage of optical micrographs from a location just under the SZ on the transverse plane (location E in Figure 1) for FSP516, illustrating the gradient in microstructure from the bottom of the SZ into the base material. The white dotted frame indicates an area scanned by OIM and summarized in Figure 6.

B. *Outside of the SZ*

1. *Beneath the center of the SZ*

Figure 5 is a montage of optical micrographs from the transverse plane at a location underneath the center of the SZ for FSP516 (location E in Figure 1). The white frame indicates the approximate area examined by OIM, and the results are shown in Figure 6. In Figure 5, a distinct interface that delineates the bottom of the SZ is apparent near the top of the montage. Just below this interface, there is a bandlike structure that is elongated in the horizontal direction and that consists of α with thin, interspersed regions of β transformation products. The banded region extends $\sim$200 μm further below the SZ/TMAZ interface, and the fraction of β transformation products decreases with the distance from the interface. At the lower center of this montage, distorted fragments of the lamellar $\alpha + \kappa_{iii}$ eutectoid constituent and deformed primary α grains are apparent. Taken together, these results indicate that the reversion reaction $\alpha + \kappa_{iii} \rightarrow \beta$ began at locations near the center of this region and so the local peak temperature was $\sim$800 °C. Globular κ_{ii} particles $\sim$20 μm in size are present throughout this montage, although distortion and elongation of the κ_{ii} particles in the direction of the SZ/TMAZ interface are apparent in locations near the interface.

Figure 6 presents a series of 100 $\times$ 100 μm^2 OIM scans obtained from the area delineated in Figure 5, and the results include IQ maps, discrete pole figures, and misorientation angle distributions. Figure 6(a) is from the location nearest the SZ/TMAZ boundary and shows a random texture like that inside the apparent SZ. The misorientation angle distribution is essentially identical to that obtained from the inside of the SZ (*i.e.,* Figure 2(c)). A single lattice orientation appears to be superimposed on a random texture at the location shown in Figure 6(b), and grain distortion is also apparent. Together, Figures 6(b) through (d) show grain distortion and lattice reorientation toward an original α grain orientation in the as-cast base metal. The reorientation appears to be concentrated in an area of $\sim$100 μm in extent around the location of Figure 6(c) and is apparent in the form of a new orientation rotated $\sim$25 deg clockwise about the *X*-axis relative to the orientation in Figure 6(b). In Figure 6(d), only the rotated orientation remains at this location under the SZ.

The inverse pole figure map for the location of Figure 6(c) is shown in Figure 7 and highlights newly recrystallized grains that have formed at this location. Comparison of these results with the OM data of Figure 5 indicates that these fine grains have formed in between two primary α grains. It is likely that many particles, *e.g.,* κ_{iv} as well as κ_{iii} due to incomplete dissolution of the lamellar eutectoid, are also present in such locations.

2. *Advancing and retreating sides*

Figure 8(a) shows a montage of optical micrographs from the plan-view plane on the advancing side of the SZ for FSP520. This plane is at about half of the SZ depth and corresponds to location F, as shown in Figure 1. The tool traversing direction is upward. Figures 8(b) through (d) show OIM results obtained from the region delineated by the dotted frame in Figure 8(a); this region spans the distinct interface between the TMAZ and SZ, and the TMAZ appears to be about 250 μm in width at this location. The OIM results are in the form of IQ maps, discrete pole figures, and misorientation angle distributions for scans that each have areas of 100 $\times$ 100 μm^2. The α grains just inside the SZ are very fine, equiaxed, and $\sim$5 μm in size in the IQ map in Figure 8(b), and the α grains are interspersed with dark-etching features that are transformation products of the β, which formed after dissolution of the eutectoid constituent. The boundary between the SZ and base metal is very sharp in the OM image of Figure 8(a), although the α (sub)grain size in the IQ maps appears to be nearly constant throughout this region. The pole figure data from locations inside the SZ/TMAZ boundary indicate a random texture, as seen in Figure 8(b), while a single lattice orientation becomes apparent upon crossing the boundary, as seen in Figure 8(c). This orientation may be interpreted as a shear texture component, $\{111\}\langle 110\rangle$, at the intersection of the

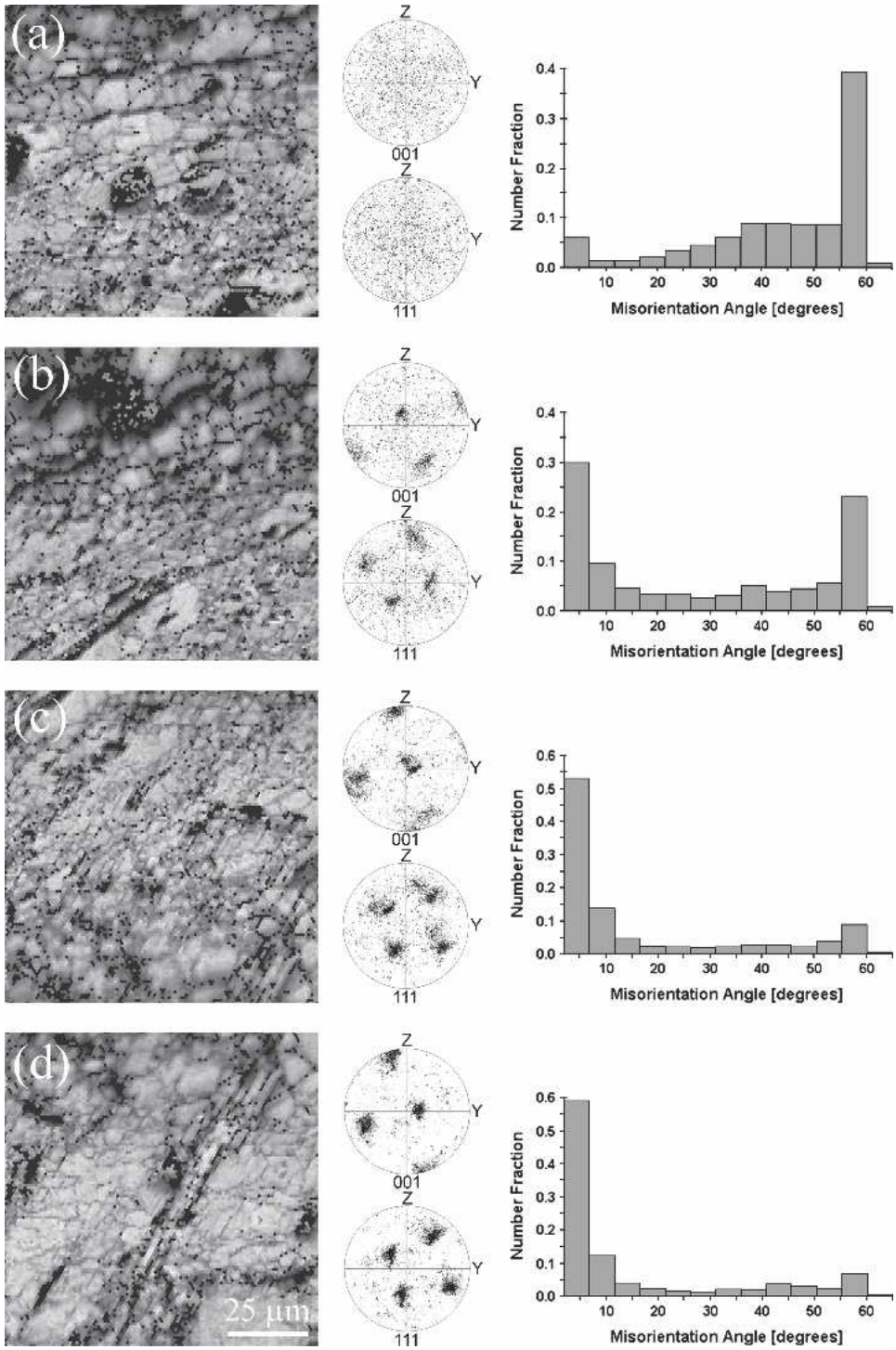

Fig. 6—A series of OIM results for region shown in Figure 5, representing IQ maps, discrete pole figures and misorientation angle distributions. The results (*a*) and (*d*) correspond to region just under the stir zone and base metal, respectively, in Figure 5.

A fiber, {111}<*uvw*>, and B fiber, {*hkl*}<110>. The notation refers to {the plane parallel to shear plane}<the direction parallel to shear direction>;[34] this interpretation requires the assumption that the strain state in the TMAZ is a simple shear on a plane approximately parallel to the local SZ/TMAZ interface and in a direction aligned with the traversing direction. In Figure 8(d), at a location farther into the TMAZ, large lattice rotation from the orientation observed in Figure 8(c) to another orientation has become apparent and the random component is less distinct. The second orientation does not correspond to a shear texture component aligned with the SZ/TMAZ interface.

Grain-to-grain misorientation angle distributions from locations inside the SZ show populations of low-angle

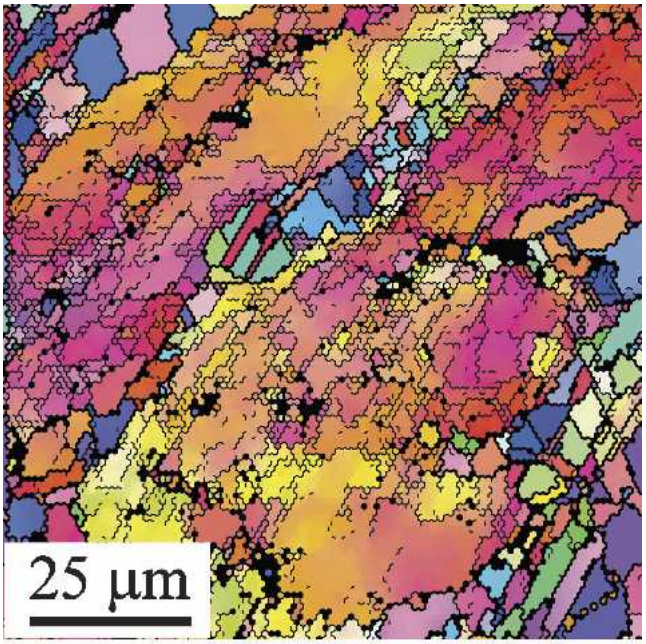

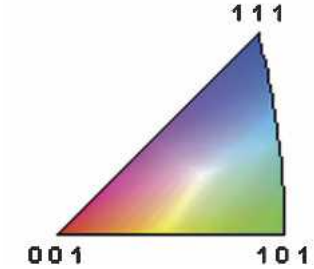

Fig. 7—The OIM results of Figure 6(c) are shown as an inverse pole figure map to highlight the newly recrystallized grains that form in between primary α grains.

and twin boundaries superimposed on an otherwise random distribution. Outside the SZ/TMAZ interface, low-angle boundaries predominate and the fraction of twin boundaries is less than inside this interface. Figure 9 is an inverse pole figure map at the location of Figure 8(c); the thin and thick lines delineate boundaries of 2 to 15 deg and boundaries of misorientation >15 deg, respectively, and show the locations of the boundaries in this region. These data suggest that an equiaxed (sub)grain structure has formed as a primary α grain has become elongated along the SZ/TMAZ interface, and that a refined grain structure may be forming as such grains become so severely elongated that capillarity effects result in fragmentation of the primary α grains.

A similar analysis was performed in the retreating side of the SZ in this material (location G, Figure 1). Figures 10(a) through (d) show a montage of optical micrographs and the OIM results, respectively. Again, the traversing direction is upward. The SZ/TMAZ boundary is less distinct on the retreating side and the TMAZ is wider than on the advancing side; in Figure 10(a), mechanical and thermal effects clearly extend over a distance of 1 mm. The TMAZ comprises distorted, bandlike regions of primary α (light etching) and β transformation products (dark etching) that are similar to the constituents noted in Figures 2(b) and 3(a) from locations within the SZ. Nevertheless, the apparent α

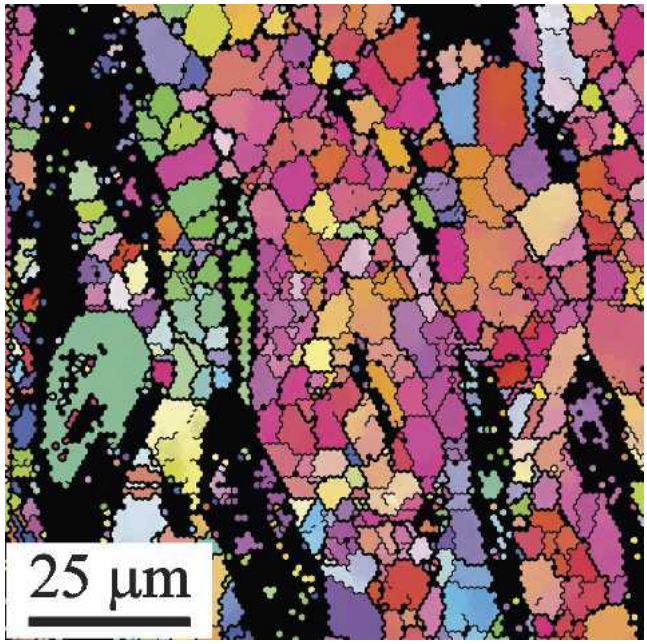

Fig. 9—The OIM results of Figure 8(c) are shown as an inverse pole figure map to highlight the newly recrystallized grains that are forming in primary α grains.

grain size is the same in all three scan areas in the IQ maps. Two shear texture components, a B-fiber orientation, {112}<110>, and an orientation at the A/B intersection, {111}<110>, are discernable in the pole figures of Figure 10(b), although both exhibit a small deviation from ideal orientations. The misorientation distribution at this location exhibits a high population of low-angle boundaries and small population of annealing twins. Only the B-fiber shear texture component is present in Figure 10(c), which is nearer the SZ. Upon approaching the SZ/TMAZ interface, the random component of the texture becomes predominant while the misorientation distributions indicate increasing populations of high-angle and twin boundaries. The shear texture component at this location may still be discerned in the pole figures of Figure 10(d), but it has become relatively faint just inside the SZ. In this region, it is likely that the intensity of shear component shows periodic variations due to the "onion-ring" structure.[35]

IV. DISCUSSION

A. *Recrystallization and Grain Refinement*

Microtexture data for the fcc α phase inside of and along the SZ periphery, *i.e.,* in the TMAZ, showed that random textures form inside the SZ, while distinct shear texture components were discernable in the TMAZ. The texture gradient was steep on the advancing side and below the SZ center, and more gradual on the retreating side. Microstructure evolution in the SZ and the TMAZ depends strongly on the strains, strain rates, and heating temperatures that are experienced during FSP. Local peak temperatures and relative cooling rates have been estimated by analysis of the constituents of the SZ microstructure in light of NAB alloy constitution.[19,20] These estimates were based

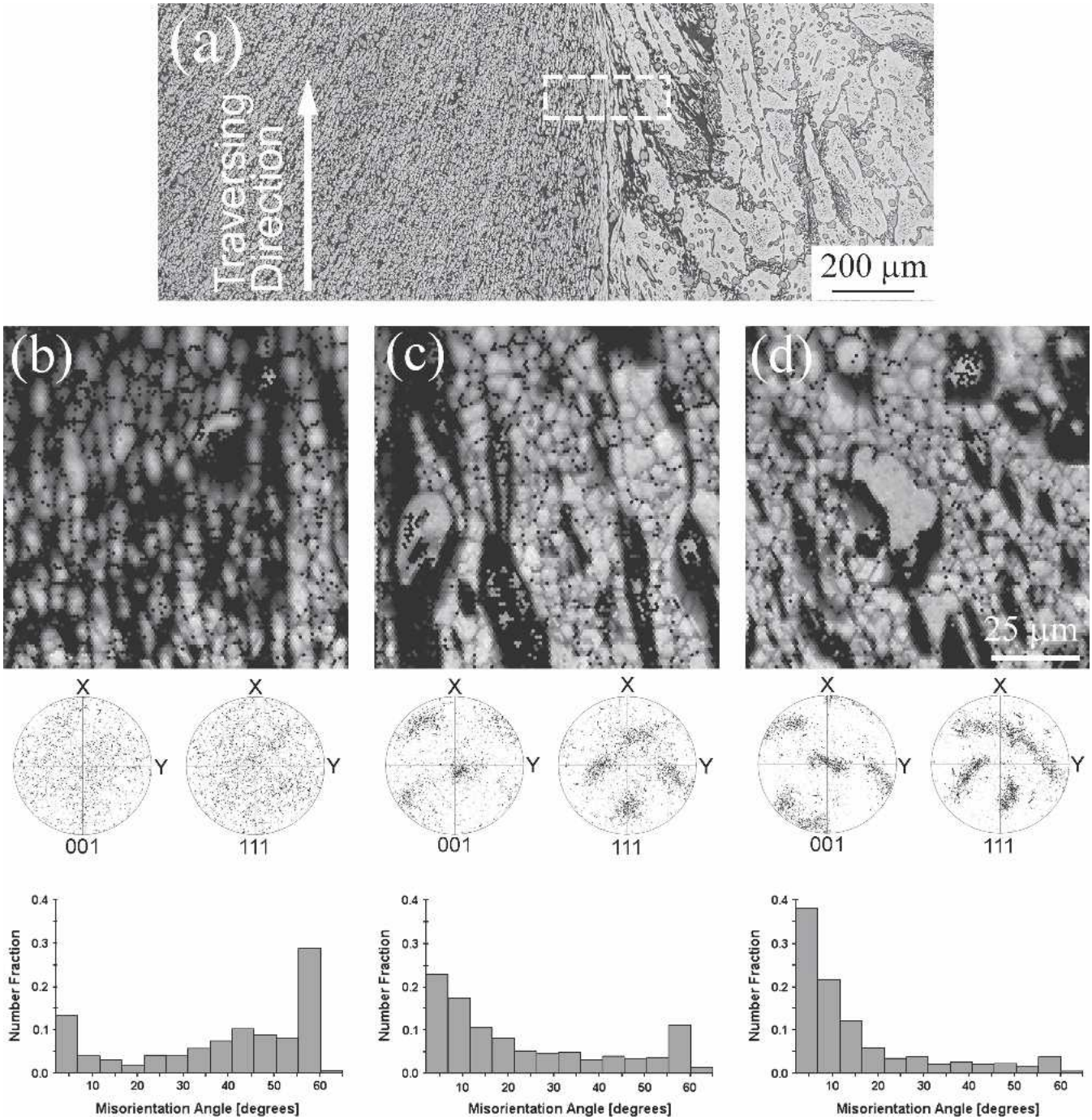

Fig. 8—(*a*) An optical micrograph; (*b*) through (*d*) show OIM results at a location on the advancing side on plan-view plane in the FSP520 sample, consisting of IQ maps, pole figures and misorientation angle distributions. The area at location (*b*) corresponds to the left side of scanned area indicated by dotted white frame in (*a*).

mainly on analysis of the nonequilibrium transformation products of β induced by FSP. Typically, SZ microstructures also include primary α that experienced deformation and annealing effects during the FSP thermomechanical cycle.

Analysis of SZ microstructures is complicated by the complex flow of material around the tool pin in addition to the steep gradients in SZ strain, strain rate, and temperature. In transverse sections, macroscopic features of SZs include not only block- and bandlike distributions of primary α and transformation products of β (*e.g.,* Figure 3(a)) but also onion-ring flow patterns.[35] The former features are often observed at locations such as A in Figure 1 and reflect compatible deformation of the α and β phases around the tool pin under the shoulder at temperatures up to ~950 °C. Often, these features appear to reflect material drawn into the SZ from the TMAZ on the retreating side. The origin of the latter features is not well understood; the onion ring patterns may reflect alternating layers of material brought together from different initial locations.

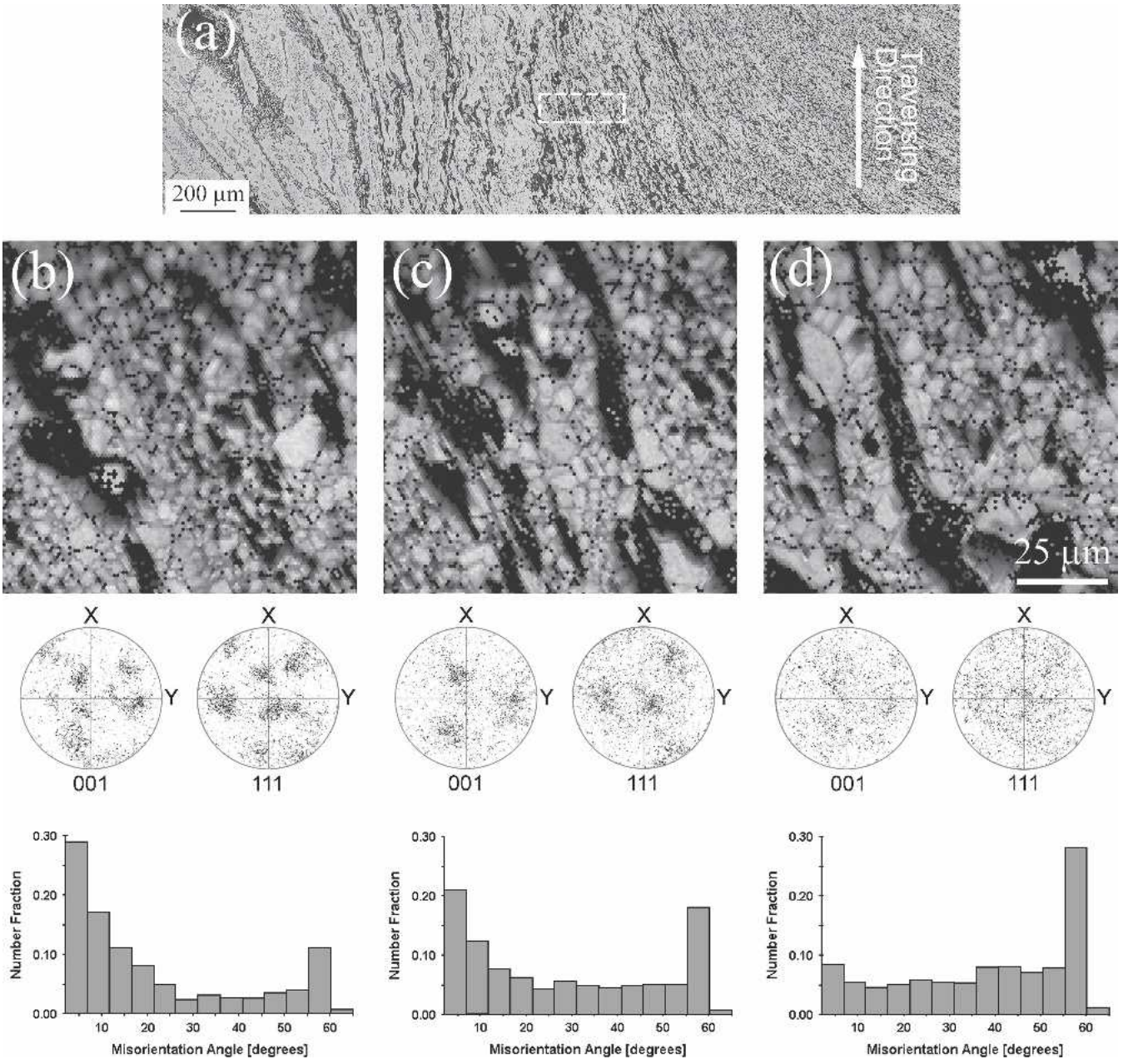

Fig. 10—(*a*) A montage of optical micrographs; (*b*) through (*d*) show OIM results at location on the retreating side on the plan-view plane (Figure 1). The OIM results are in the form of IQ maps, misorientation angle distributions and discrete (001) and (111) pole figures and were obtained from the area delineated by the dotted white frame in (*a*); the TMAZ is to the left and the SZ is to the right.

Nevertheless, refined α grains and random α phase textures are apparent irrespective of SZ location. Furthermore, α phase grain-to-grain misorientation angle distributions comprise superposition of random and annealing twin populations. In regions of the SZ near the tool shoulder, populations of low-angle boundaries were observed despite the absence of deformation texture components, which suggests that only small strains occurred after formation of new grain orientations. It has been noted that many previous studies of FSW/P of Al alloys have shown that fine grains form but distinct shear textures persist throughout weld nuggets or SZs.[24–26,31] Such microstructures and textures have been ascribed to continuous dynamic recrystallization involving the formation of new grains by dislocation reaction in the deformation microstructure in the absence of the long-range migration of high-angle boundaries.[36] Such processes typically involve retained deformation textures; random SZ α phase textures suggest that alternative recrystallization mechanisms occur during FSP of these NAB materials.

The equilibrium-cooled as-cast NAB material here consists of coarse primary α grains containing κ_{iv} particles ~1 to 10 μm in size, and the lamellar $\alpha + \kappa_{iii}$ eutectoid constituent containing globular κ_{ii} particles up to ~20 μm in size. The SZ microstructures and microstructure-based estimates of local SZ temperature indicate the temperature at the

SZ/TMAZ interface is ~800 °C and that severe deformation begins as the local temperature exceeds this value upon tool approach to a location along its path. At this temperature, κ_{iv} particles up to ~10 μm in size will persist in the α grains, although these particles likely will also undergo spheroidization and coarsening. Still, severe deformation will generate localized deformation zones around these particles. For lattice-diffusion control of deformation and recovery, the strain rate necessary to achieve particle-stimulated nucleation (PSN) of recrystallization is given by[37]

$$\dot{\varepsilon}_{\mathrm{PSN}} \geq \frac{K_1}{d_p^2 T} \exp\left(-\frac{Q_D}{\mathrm{k}T}\right) \qquad [1]$$

where $K_1 = \frac{\Omega G D_{0,l}}{\mathrm{k}}$. In these relationships, Ω is the atom volume, G is the shear modulus, $D_{0,l}$ is the pre-exponential factor for lattice diffusion, k is the Boltzmann's constant, d_P is the particle diameter, T is the temperature, and $Q_{D,l}$ is the activation energy for lattice diffusion. When the local strain rate is sufficient to satisfy Eq. [1], local lattice rotations will lead to the formation of deformation zones around particles and support nucleation of new grains at the particles. Lattice-diffusion control may be assumed because of the high local temperatures, and, so, terms involving boundary diffusion have been omitted from Eq. [1]. For Cu, $\Omega = 1.18 \times 10^{-29}$ m^3, $G = 42$ GPa, and $D_{0,l} = 0.3 \times 10^{-4}$ m^2 s^{-1}, so that $K_1 = 0.913$ m^2 K s^{-1}; also, $Q_D = 197$ kJ mol^{-1}.[38] Taking $d_p \sim 5$ μm for the κ_{iv} particles (the middle of the observed range of particle sizes) and the temperature $T = 800$ °C at the SZ/TMAZ interface, the strain rate for PSN is $\dot{\varepsilon}_{\mathrm{PSN}} = 9 \times 10^{-3}\,\mathrm{s}^{-1}$. Modeling has indicated that $\dot{\varepsilon}_{\mathrm{local}} \approx 200\,\mathrm{s}^{-1}$ in the SZ near the pin surface during FSP of NAB materials;[39] the process is characterized by steep gradients in strain rate and temperature, and so PSN is a plausible mechanism for recrystallization in the primary α at the SZ/TMAZ interface at locations where the κ_{iv} particles persist in the microstructure. Typically, PSN results in random lattice orientations of the recrystallized grains due to the random nature of the local lattice reorientations in the deformation zones around the particles and this would account for the random textures nearby the SZ/TMAZ interface in the lower SZ.

The finest primary α grain size was observed at the SZ/TMAZ interface. At locations further inside the SZ, the κ_{iv} particles will inhibit grain growth until the local peak temperature attains ~860 °C. Above this temperature, the κ_{iv} particles will dissolve completely and grain growth may then occur in the primary α. However, the lamellar $\alpha + \kappa_{iii}$ will commence reversion to form to β as the temperature exceeds ~800 °C, and, as the volume fraction of β increases with heating temperature above 800 °C, it will retard the α grain growth. The κ_{ii} phase persists to ~930 °C, but the size and dispersion both are coarse, and, so, it will be less effective in the inhibition of grain growth in the primary α. As peak temperatures during FSP are often 860 °C to 930 °C, microstructures will consist of primary α that has experienced recrystallization, and transformation products of the β. This is typically seen in the middle to upper regions of the SZ, *e.g.,* as shown in Figure 2(b), and the random α phase textures reflect persistence of random orientations developed by PSN during rapid heating and severe deformation prior to attaining peak temperature. The α/β interfaces may also become sites for recrystallization initiation during severe deformation in the $\alpha + \beta$ two-phase region, but textures associated with such a reaction have not been separately identified in materials such as this NAB composition.

Region A (Figure 2(a)) represents material nearby the plate surface in contact with the tool shoulder, and this material has the highest fraction of low angle boundaries, $\theta < 15$ deg, in the SZ grain-to-grain misorientation distributions. For higher misorientation angles, *i.e.,* $\theta > 15$ deg, the distributions are essentially identical for all SZ locations (*i.e.,* regions B through D; and inside the SZ at G and F). The tool shoulder diameter is about three times the pin diameter, and, so, the upper SZ will continue to experience deformation by the shoulder after passage of the pin. For FSP516 (Table I), the peak temperature near the surface was estimated to be ~930 °C,[19] *i.e.,* ~$0.9T_M$. At this temperature, recovery of dislocations introduced by deformation due to the tool shoulder and additional deformation due to the build up of residual stresses during the cooling will result in subgrain formation. Thus, the higher population of low-angle boundaries in the upper SZ reflects a combination of dynamic recovery during deformation by the tool shoulder and static recovery during subsequent cooling. It is possible that static recovery effects and steep microstructure gradients may also account for the relatively large population of low-angle boundaries inside the SZ on the advancing side.

B. *Texture in the SZ and TMAZ*

Deformation textures were observed in the TMAZ around the periphery of the SZ. Under the center of the SZ, lattice rotation is accompanied by shearing distortion of the grains, and the local lattice orientation may be interpreted in terms of simple shear on a plane approximately parallel to the local plane of the SZ/TMAZ interface. Shear texture components are apparent in the TMAZ on the advancing and retreating sides, while the texture gradient from the base metal to the SZ is steeper on the advancing side than on the retreating side. A correspondingly steeper gradient in microstructure on the advancing side is apparent when Figure 8(a) is compared to Figure 10(a). The misorientation distributions in the TMAZ include high populations of low-angle boundaries in locations that exhibit relatively small deformations of the primary α grains and recovery during cooling after passage of the tool.

The deformation textures and large low-angle boundary populations in the TMAZ change rapidly upon crossing the SZ/TMAZ interface and both the textures and misorientation distributions reflect mainly random SZ grain orientations. In contrast, Al alloys exhibit fine, equiaxed grains accompanied by deformation-induced shear textures that become evident in the TMAZ and persist to the centers of the weld nuggets following FSW.[24–26,31] The presence of shear texture orientations has been cited as evidence that microstructures evolve by recovery-dominated dynamic continuous recrystallization in FSW/P of aluminum alloys in contrast to the PSN reaction during FSP of this NAB material.

A shear texture component corresponding to the intersection of A- and B-type shear texture fibers was identified

in the TMAZ on both the advancing and retreating sides, while an additional B-type shear texture orientation was observed at locations on the retreating side. Ideal orientations for each of these components are illustrated by 111 stereographic projections in the upper schematic of Figure 11. These projections reflect ideal orientations represented in the *X-Y* plane for shear in the *X* direction on a plane parallel to a SZ/TMAZ interface. In turn, the shear plane for these projections has been assumed to coincide with the *X-Z* plane in this diagram, *i.e.,* it is perpendicular to the plane of the diagram in the upper schematic of Figure 11. The actual SZ/TMAZ interface is inclined to the *X-Z* plane by an angle that varies with location along the SZ/TMAZ interface. This is indicated in a transverse section in the schematic of the lower diagram of Figure 11, in which the trace of the shear plane is inclined to the plate surface by an angle at a position along the SZ/TMAZ interface. In the ideal case, a {111} will tend to be perpendicular to the plate surface and parallel to the traversing direction for the A/B intersection component, while a {111} is tilted about 20 deg from the tool axis (*Z*-axis) for the B-fiber component. Similar results have been reported by Sato *et al.*,[24] who have reported characteristic shear texture components with two orientations, each of which have a common {111} and <110> roughly parallel to the pin surface and the traverse direction of the plate (the *Y*-axis here) in AA6063 at a midsection location at the weld center. These orientations were attributed to initial deformation associated with the tool pin and they subsequently became inclined ~20 deg from the *X*-axis toward the *Z*-axis due to severe stresses arising from the tool shoulder upon passage of the tool pin. Also, the dominant shear direction was everywhere aligned with the tangent to the rotating tool, and a prominent {111} orientation is oriented 70 deg away from plate normal from immediately under the shoulder to the midplane of a weld.[25] Furthermore, Park *et al.*[11,27] have applied FSW to hcp Mg in which slip occurs preferentially on the {0002} basal plane, which was shown to align with an ellipsoidal surface in the nugget-shaped SZ. In the friction-stir-processed NAB material, the B fiber is evidently the dominant shear texture orientation in the TMAZ (the A/B intersection is at one end of the B fiber). Therefore, the shear textures have a common <110> shear direction that tends to align with the traversing direction. Then, it is likely that a {111} tends to align with the local plane of the SZ/TMAZ interface.

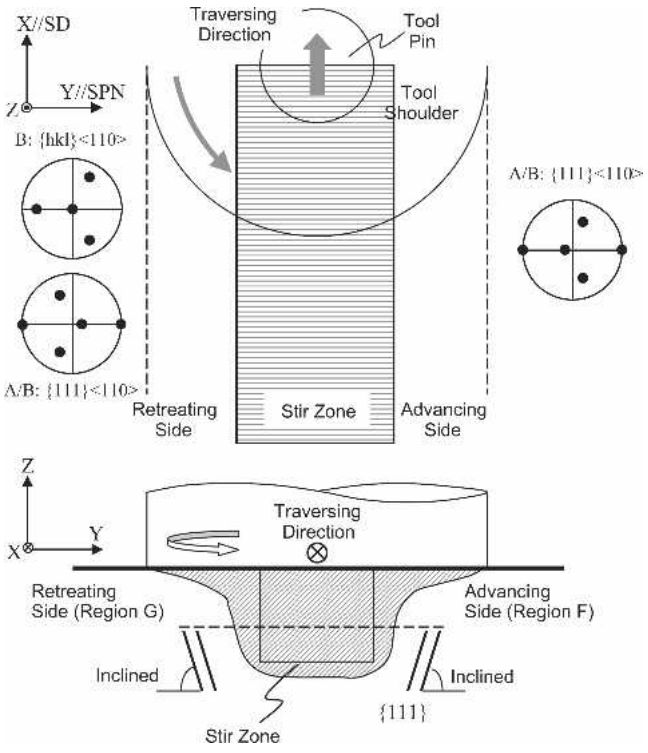

Fig. 11—Schematic diagrams of the plan-view plane at half the depth of the SZ (the upper diagram) and the transverse plane (lower diagram), showing characteristic lattice orientations in the TMAZ around the periphery of the SZ in the form of stereographic projections. The projections show orientations in the planes of observation for a local shear plane aligned with the local SZ/TMAZ interface and with a local shear direction aligned with the tool traversing direction.

V. CONCLUSIONS

1. Random α phase textures are apparent throughout the SZ, reflecting the predominance of recrystallization by PSN at the various κ-phase constituent particles that are retained during the rapid heating and straining of FSP. The α/β interface in the duplex structure developed at $T \geq 800$ °C may also provide nucleation sites for recrystallization.
2. The population of subgrain boundaries in α-phase grains is highest near the plate surface in contact with the tool where the α phase grain size is ~10 μm. The population of subgrain boundaries and the α-phase grain size both decrease with the depth in the SZ. Subgrain formation is most pronounced near the plate surface due to the effect of deformation by the tool shoulder after the passage of the tool pin.
3. The PSN of recrystallization results in α phase grains 1 to 2 μm in size at the bottom of the SZ. Such locations experience severe deformation at temperatures in the vicinity of the eutectoid temperature of 800 °C and the grain size is refined by a factor of 10^3 in such locations when comparison is made to the as-cast material.
4. Annealing twins are observed throughout the SZ.
5. Shear texture components are resolvable in the TMAZ just outside of the SZ. The shear texture component {111}<110> (A/B intersection), where {*hkl*} is the shear plane and <*uvw*> is the shear direction, was observed on the advancing side. A {112}<110> (B-type) component and {111}<110> were observed on the retreating side.
6. The shear texture components observed in present study all have a common shear direction, <110>, which is aligned with the traversing direction of FSP. The shear plane generally tends to align with the local plane of the interface between the TMAZ and SZ.

ACKNOWLEDGMENTS

The authors acknowledge the provision of FSP materials by Mr. Murray Mahoney, Rockwell Scientific Corporation.

The Naval Surface Warfare Center (Carderock, MD) supplied the NAB material, and the Defense Advanced Research Projects Agency (DARPA), with Dr. Leo Christodoulou as program sponsor, provided funding for this work.

REFERENCES

1. W.M. Thomas, E.D. Nicholas, J.C. Needham, M.G. Murch, P. Templesmith, and C.J. Daws: G.B. Patent Application No. 9125978.8, Dec. 1991; U.S. Patent No. 5460317, Oct. 1995.
2. R.S. Mishra: *Adv. Mater. Processes*, 2003, vol. 161 (10), pp. 43-46.
3. R.S. Mishra, Z.Y. Ma, and I. Charit: *Mater. Sci. Eng. A*, 2003, vol. A341, pp. 307-10.
4. Z.Y. Ma, R.S. Mishra, and M.W. Mahoney: in *Friction Stir Welding and Processing II*, K.V. Jata, M.W. Mahoney, R.S. Mishra, S.L. Semiatin, and T. Lienert, eds., TMS, Warrendale, PA, 2003, pp. 221-30.
5. R.S. Mishra, M.W. Mahoney, S.X. McFadden, N.A. Mara, and A.K. Mukherjee: *Scripta Mater.*, 2000, vol. 42, pp. 163-68.
6. R.S. Mishra and M.W. Mahoney: in *Superplasticity in Advanced Materials – Proc. ICSAM2000*, N. Chandra, ed., Materials Science Forum, Trans Tech Publications, Aedermannsdorf, Switzerland, 2001, vols. 357–359, pp. 507-14.
7. Z.Y. Ma, R.S. Mishra, and M.W. Mahoney: *Acta Mater.*, 2002, vol. 50, pp. 4419-30.
8. I. Charit and R.S. Mishra: *Mater. Sci. Eng., A*, 2003, vol. A359, pp. 290-96.
9. Z.Y. Ma, R.S. Mishra, M.W. Mahoney, and R. Grimes: *Mater. Sci. Eng. A*, 2003, vol. A351, pp. 148-53.
10. Y.S. Sato, M. Urata, and H. Kokawa: *Metall. Mater. Trans. A*, 2002, vol. 33A, pp. 625-35.
11. S.H.C. Park, Y.S. Sato, and H. Kokawa: *Scripta Mater.*, 2003, vol. 49, pp. 161-66.
12. D. Zhang, M. Suzuki, and K. Maruyama: *Scripta Mater.*, 2005, vol. 52, pp. 899-903.
13. H.S. Park, T. Kimura, T. Murakami, Y. Nagano, K. Nakata, and M. Ushio: *Mater. Sci. Eng., A*, 2004, vol. A371, pp. 160-69.
14. Y.S. Sato, T.W. Nelson, and C.J. Sterling: *Acta Mater.*, 2005, vol. 53, pp. 637-45.
15. A.P. Reynolds, E. Hood, and W. Tang: *Scripta Mater.*, 2005, vol. 52, pp. 491-94.
16. M.W. Mahoney, W.H. Bingel, S.R. Sharma, and R.S. Mishra: *Mater. Sci. Forum*, 2003, vol. 426-4, pp. 2843-48.
17. K. Oh-ishi, A.P. Zhilyaev, R. Williams, and T.R. McNelley: in *Friction Stir Welding and Processing III*, K.V. Jata, M.W. Mahoney, R.S. Mishra, and T.J. Lienert, eds., TMS, Warrendale, PA, 2005, pp. 107-14.
18. I. Charit and R.S. Mishra: *Acta Mater.*, 2005, vol. 53, pp. 4211-23.
19. K. Oh-ishi and T.R. McNelley: *Metall. Mater. Trans. A*, 2004, vol. 35A, pp. 2951-61.
20. K. Oh-ishi and T.R. McNelley: *Metall. Mater. Trans. A*, 2005, vol. 36A, pp. 1575-85.
21. J.L. Robbins, O.C. Shepard, and O.D. Sherby: *J. Iron Steel Inst.*, 1964, vol. 202, pp. 804-07.
22. O.D. Sherby, B. Walser, C.M. Young, and E.M. Cady: *Scripta Metall.*, 1975, vol. 9, pp. 569-74.
23. B. Walser and O.D. Sherby: *Metall. Trans. A*, 1979, vol. 10A, pp. 1461-71.
24. Y.S. Sato, H. Kokawa, K. Ikeda, M. Enomoto, S. Jogan, and T. Hashimoto: *Metall. Mater. Trans. A*, 2001, vol. 32A, pp. 941-48.
25. D.P. Field, T.W. Nelson, Y. Hovanski, and K.V. Jata: *Metall. Mater. Trans. A*, 2001, vol. 32A, pp. 2869-77.
26. R.W. Fonda, J.F. Bingert, and K.J. Colligan: *Scripta Mater.*, 2004, vol. 51, pp. 243-48.
27. S.H.C. Park, Y.S. Sato, and H. Kokawa: *Metall. Mater. Trans. A*, 2003, vol. 34A, pp. 987-94.
28. P. Brezina: *Int. Met. Rev.*, 1982, vol. 27, pp. 77-120.
29. F. Hasan, A. Jahanafrooz, G.W. Lorimer, and N. Ridley: *Metall. Trans. A*, 1982, vol. 13A, pp. 1337-45.
30. A. Jahanafrooz, F. Hasan, G.W. Lorimer, and N. Ridley: *Metall. Trans. A*, 1983, vol. 14A, pp. 1951-56.
31. P.B. Prangnell and C.P. Heason: *Acta Mater.*, 2005, vol. 53, pp. 3179-92.
32. J.K. MacKenzie: *Biometrika*, 1958, vol. 45, pp. 229-40.
33. V. Randle and O. Engler: *Introduction to Texture Analysis: Macrotexture, Microtexture & Orientation Mapping*, Gordon and Breach, Amsterdam, The Netherlands, 2000, pp. 138 and 226.
34. G.R. Canova, U.F. Kocks, and J.J. Jonas: *Acta Metall.*, 1984, vol. 32, pp. 211-26.
35. K.N. Krishnan: *Mater. Sci. Eng., A*, 2002, vol. 327, pp. 246-51.
36. R.D. Doherty, D.A. Hughes, F.J. Humphreys, J.J. Jonas, D. Juul-Jensen, M.E. Kassner, W.E. King, T.R. McNelley, H.J. McQueen, and A.D. Rollett: *Mater. Sci. Eng., A*, 1997, vol. A238, pp. 219-74.
37. F.J. Humphreys: *Acta Metall.*, 1977, vol. 25, pp. 1323-44.
38. J. Askill: *Tracer Diffusion Data for Metals, Alloys and Simple Oxides*, IFI Plenum, New York, NY, 1970, pp. 32-45.
39. A. Askari, S. Silling, B. London, and M.W. Mahoney: in *Friction Stir Welding and Processing*, K.V. Jata, M.W. Mahoney, R.S. Mishra, S.L. Semiatin, and D. P. Fields, eds., TMS, Warrendale, PA, 2001, pp. 43-50.